Proceedings of 4th National Applied Mechanisms and Robotics Conference, December 95

Optimal Traction Control In A Wheelchair With Legs And Wheels

Venkat Krovi
Research Associate

Vijay Kumar
Associate Professor

Department of Mechanical Engineering
University of Pennsylvania
Philadelphia, Pennsylvania 19104-6315

ABSTRACT

We propose a proof-of-concept prototype wheelchair with legs for people with motor disabilities with the objective of demonstrating the feasibility of a completely new approach to mobility. Our prototype system is a vehicle equipped with powered wheels and legs and is capable of traversing uneven terrain and circumventing obstacles such as steps and ditches. The design combines the advantages of legged locomotion (versatility, adaptability) with wheeled locomotion (reliability, superior stability). When the wheels and legs are employed together, the system is redundantly actuated. In this paper, we describe a coordination scheme that allows us to optimize the tractive capabilities of the vehicle. The basic underlying idea is to minimize the tendency of the wheels and legs to slip. This is accomplished by minimizing the largest friction angle at all the locomotion elements. We briefly describe our experimental prototype. Simulation and experiments are used to demonstrate the performance of the active traction optimization scheme.

INTRODUCTION

Motorized wheelchairs with sophisticated controls are available for people with disabilities. While they can locomote on prepared surfaces most are unable to surmount common obstacles like steps and curbs [11]. (See ANSI/RESNA WC/10 or ISO 7176/10 standards for determination of the obstacle climbing ability of a wheelchair). Architectural modifications such as curb cuts, ramps and elevators improve accessibility but are primarily limited to new buildings [7]. Wheelchair users often cannot enjoy strolling on beaches nor can they easily cross muddy patches and potholes. Previous research in rehabilitation engineering has concentrated primarily on constructing a better wheelchair [5,9,15,16]. Many special purpose aids including stair climbers and customized outdoor buggies have been developed to solve specific problems [5,13,15] but they tend to be customized to a particular environment and are not versatile.

A legged vehicle allows locomotion in environments cluttered with obstacles where wheeled or tracked vehicles cannot be used. It is inherently omni-directional, provides superior mobility in difficult terrain or soil conditions (sand, clay, gravel, rocks etc.) and provides an active suspension. The legs also give the chair versatility and allow it to be re-configured. When stationary, one of the legs can be used as a manipulator in order to perform simple tasks such as reaching for objects or pushing open doors.

In the past two decades, several articulated legged vehicles have been designed and built in research laboratories. Most work has focused on *statically stable* locomotion, characteristic of insects [17], in which the legs maintain the vehicle in static equilibrium. This is contrasted with *dynamically stable locomotion* [12] that is exhibited by galloping four-legged animals and walking (or running) humans. A number of proof-of-concept statically stable legged robots have been built [2,8,10,17]. Although they are more reliable and are likely to be more acceptable to consumers than dynamically stable machines, they are still suffer from one major disadvantage. It is difficult to achieve the required strength/weight ratio using conventional actuators. With a payload of 100 kgs, if we assume a maximum vehicle weight of as much as 100 kgs (net weight = 200 kgs) for a four-legged vehicle, each leg must be able to support a minimum of 100 kgs (in addition to providing the tractive force). This translates to a payload/weight ratio of over 4 for each leg. It is difficult to design a moderately-expensive, compact actuation system with such stringent requirements. By increasing the number of legs, the required strength/weight ratio becomes smaller but the design becomes less compact. Further our informal survey of potential consumers indicated that a four-legged walking chair [20] is likely to suffer from a lack of acceptance by consumers.

In a conventional wheeled system, the payload is supported passively while the actuation system only has to provide the tractive force. Motivated by this observation we considered an alternative design that combines the advantages of legged locomotion (versatility, adaptability) with wheeled locomotion (reliability, superior stability). Our prototype of such a *hybrid* vehicle with four wheels (two powered) and two legs is shown in Figure 1. Such a *hybrid* vehicle is capable of using powered wheels to navigate on a flat surface with relatively low actuator forces/torques. The legs are used primarily on uneven terrain and on unprepared surfaces. A maneuver similar to walking is accomplished by using the legs to drag the vehicle forward or push backward. The legs are used with wheels to provide additional traction on slippery surfaces. Alternative uses include use as manipulators, to push open doors or move obstacles.

When the wheels and legs are used in conjunction, the system is statically indeterminate. Because we actively

control the wheels and legs, it is necessary to resolve this actuator redundancy [6]. In this paper, we describe a coordination scheme that allows us to optimize the tractive capabilities of the vehicle. This is accomplished by minimizing the largest friction angle at all the locomotion elements. We briefly describe our experimental prototype. Simulation and experiments are used to demonstrate the performance of the active traction optimization scheme.

THE PROTOTYPE SYSTEM

A picture of the prototype is shown in Figure 1 while the essential mechanical details are shown in a CAD model in Figure 2. The two 12 volt batteries, the amplifiers and the controller are not shown in the figures. The prototype weighs 62 lbs (28.2 kgs), not including the controller and batteries. The prototype is 28 inches wide and can go through a standard 30 inch doorway. The rear wheel radius is 4.25 inches while the wheelbase is 20 inches.

FIG 1: THE EXPERIMENTAL PROTOTYPE.

Each leg is a 2*R* linkage driven by two motors that are mounted on the chassis in a parallel-drive configuration [14] in which power is transmitted to the distal link through a chain and sprocket transmission. Each link is 16 inches long giving the leg a net reach of approximately 32 inches (0.81 m). The chain is preloaded to remove backlash. At the end of the distal link is a compliant ankle which is a linear spring loaded joint on linear bearings.

Each joint in the leg is driven by a DC gear motor (PMI 12FG) capable of exerting 200 in-lbs (22.6 N-m) of torque at 26 rpm, with a peak (stall) torque of 240 in-lbs. (27.12 N-m). A further external speed reduction of 3:1 is accomplished between the gear motor and the link. Each rear wheel is driven by a similar, smaller gear motor (PMI 9FG) with a rating of 40 in-lbs (4.5 N-m) continuous torque. At the rated wheel speed (78 rpm), the chair can move at 0.93 meters/second (3.4 km/hour). All motors (legs and wheels) are mounted on the chassis (base of the chair) so that their weight is not borne by the moving links as can be seen in Figure 2 below.

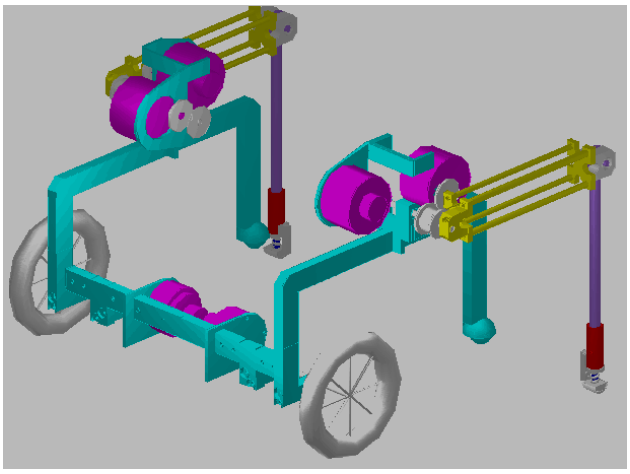

FIG 2: AN AUTOCAD MODEL OF THE SYSTEM.

The motors are driven by 20 kHz PWM switching amplifiers (Kollmorgen VXA 48-8-8) that operate off of a 24 Volt DC source. Although in the laboratory we use transformers and AC line voltage, the vehicle can be operated on two standard 12 volt lead acid batteries with a peak current requirement of 6 amperes. The amplifiers are configured to clamp to the motor current determined by the control signals received from the control computer. System feedback is achieved using a 500 line resolution incremental optical encoders also supplied by Kollmorgen/ PMI. Because of the gearing, the encoders provide a resolution of 2500 counts per degree of joint shaft rotation for each leg. Position is measured directly from the encoders that are mounted on the input side of each motor and the velocity is computed digitally by taking successive derivatives of the position signal. A digital I/O card (Keithley Metrabyte DDA 06) is used for data acquisition.

The tension in the chain is sensed by strain gages mounted on the chain. This facilitates the measurement of the applied torque on the distal link. A force plate using folded back cantilever beams instrumented with strain gages is used to measure the vertical reaction force exerted by the distal link at the foot. The Signal Conditioning Amplifier (Analog devices, 3B18) is mounted close to the gages to minimize noise. A data acquisition card (Real Time Devices, ADA2000) is used to convert the analog strain measurements. The applied tangential force at the foot is inferred from this combination of sensors using the inverse kinematics map.

The control computer is an IBM compatible 486 machine with an i860 processor running in parallel. The i860 is used to perform the control computations that are necessary to process the sensory data and coordinate the multiple actuators. The 486 processor performs all system input and output tasks.

More details on the mechanical design and the system integration are available from references [18,19].

MATHEMATICAL MODELING

We analyze the planar wheelchair system in the sagittal plane with the variables as assigned in Figure 3. We assume rolling contacts between the ground and the mechanism both at the foot and at the wheel. The system is redundantly described by the following 6×1 vector of Lagrangian coordinates.

$$q = \left[x_w, y_w, \theta_1, \theta_2, \theta_3, \theta_4\right]^T \tag{1}$$

where $x_w, y_w, \theta_1, \theta_2, \theta_3, \theta_4$ are defined in the table below.

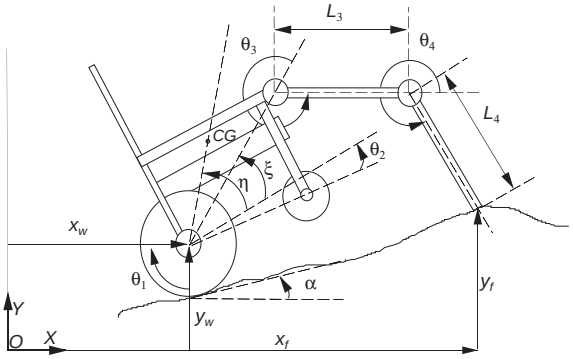

FIG 3: THE VARIABLES ASSIGNED TO THE CHAIR.

VARIABLE	DESCRIPTION
O,XY	Inertial global frame.
CG	Center of Gravity of Chair.
α	Angle between tangent to the ground and the X-axis.
x_f	X Coordinate of the foot contact.
y_f	Y Coordinate of the foot contact.
x_w	X coordinate of the wheel axle.
y_w	Y coordinate of the wheel axle.
M_c	Distance of CG from the wheel axle.
η	Included angle between CG and base level of the chair.
N_c	Distance of arm attachment from the wheel axle.
ξ	Included angle arm attachment and base level.
L_3	Length of the upper limb.
L_{3c}	Distance of c.g. of upper limb from the proximal joint.
L_4	Length of the lower limb.
L_{4c}	Distance of c.g. of lower limb from the distal joint.
θ_1	Rotation of the wheel.
θ_2	Chair lift angle (angle between base level and ground).
θ_3	Relative angle between link3 and link2.
θ_4	Relative angle between link4 and link3.

TABLE 1: SYMBOL TABLE OF SYMBOLS USED IN THE FORMULATION.

KINEMATICS

The inverse kinematics computation for the mechanism is unique and is computed analytically. A nonlinear system of equations Eq.2-5 is set up with the four known quantities. They are the expressions for the Cartesian position of one point on the chair (e.g. the center of mass x_{cg} and y_{cg}) and the Cartesian position of the tip of the foot (x_f and y_f).

$$x_{cg} = R\,\theta_1\,C_\alpha - R\,S_\alpha + M_c\,C_{\alpha\eta 2} \tag{2}$$

$$y_{cg} = R\,\theta_1\,S_\alpha + R\,C_\alpha + M_c\,S_{\alpha\eta 2} \tag{3}$$

$$x_f = R\,\theta_1\,C_\alpha - R\,S_\alpha + N_c\,C_{\alpha\xi 2} + L_3\,C_{\alpha\xi 23} + L_4\,C_{\alpha\xi 234} \tag{4}$$

$$y_f = R\,\theta_1\,S_\alpha + R\,C_\alpha + N_c\,S_{\alpha\xi 2} + L_3\,S_{\alpha\xi 23} + L_4\,S_{\alpha\xi 234} \tag{5}$$

where $C_{\alpha\beta\mathrm{L}\,\delta} = Cos(\alpha+\beta+\mathrm{L}+\delta)$

and $S_{\alpha\beta\mathrm{L}\,\delta} = Sin(\alpha+\beta+\mathrm{L}+\delta)$.

For any given x_{cg}, y_{cg}, x_f and y_f the solution of this set of equations yields analytic solutions for the angles $\theta_1 \ldots \theta_4$.

A quick analysis, using the Gruebler criterion, shows that the system has only two degrees of freedom. Since we have used six Lagrangian variables to describe the system we also specify four equations of constraint. The constraints can be holonomic or nonholonomic. In the planar case we have four holonomic constraints. However, in general, we have two holonomic and two nonholonomic constraints.

The holonomic constraints arise out of the impenetrability / high stiffness of rigid body contact and the non holonomic constraints arise from the no slip condition imposed on the wheels. Here, for the sake of generality, we differentiate the holonomic constraints and use all the constraints in the differential form.

The choice of surplus coordinates and constraints in the formulation becomes clear here. We now have explicit analytical expressions for the reaction forces at the wheel and the foot (in the form of Lagrange multipliers) which will be used in the formulation. We can now write the matrix differential form of the constraint as,

$$A(q)\dot{q} = 0 \tag{6}$$

We then determine a 6×2 full rank matrix $S(q)$ as the null space of the constraint matrix expressed in the differential form as follows,

$$A(q)S(q) = 0 \tag{7}$$

The columns of S span the motion space of the constrained system. It is now possible to define two generalized velocities,

$$v = \left[v_1, v_2\right]^T \tag{8}$$

which completely describe the motion at the velocity level. The general solution to Eq.6 can now be written as,

$$\dot{q} = S(q)\,v(t) \tag{9}$$

which can be written in the acceleration level as,

$$\ddot{q} = S(q)\,\dot{v}(t) + \dot{S}(q)\,v(t) \tag{10}$$

DYNAMICS

The dynamic equations of a constrained mechanical system are written as,

$$M(q)\,\ddot{q} + h(q,\dot{q}) = E(q)\,\tau \; - A^T\,\sigma \tag{11}$$

$$A(q)\,\dot{q} = 0$$

where, M is the 6×6 generalized inertia matrix, $\ddot{q}$ is the 6×1 acceleration vector, h is the 6×1 vector of nonlinear and gravity terms, τ is the 3×1 vector of torques applied to the system, λ is the 4×1 vector of Lagrange multipliers and E is the 6×3 actuator distribution matrix for the generalized coordinates.

Multiplying Eq.11 by S^T and substituting from Eq.9-10 we get,

$$\dot{v} = -(S^T M S)^{-1}\left[\left(S^T M \dot{S} v + S^T h\right) - S^T E \tau\right] \quad (12)$$

Inverting the 6×6 positive definite symmetric matrix M in Eq.11 we get,

$$\ddot{q} = M^{-1}\left[E\tau - A^T \sigma - h\right] \quad (13)$$

Differentiating Eq.6 and substituting from Eq.13 yields,

$$\lambda = (AM^{-1}A^T)^{-1}\left[\dot{A}Sv - AM^{-1}h + AM^{-1}E\tau\right] \quad (14)$$

TRACTION OPTIMIZATION

We note that in Eq.12 while q, v, and $\dot{v}$ are known from the desired trajectory we have three unknowns (actuator torques) and only two equations. Thus, the requirement for an additional criterion arises because of redundancy in actuation (due to the formation of the closed loop).

A variety of criteria have been proposed in the past. We choose to adopt the criterion proposed by [21] because we would like to minimize the tendency to slip at the wheels and at the feet. We achieve this by minimizing the largest friction angle at all the contact point.

We define the *force ratio* (r_i) at each contact as the ratio of the tangential force to the normal force, normalized by the friction coefficient μ as shown below,

$$r_i = \left[F_{t,i}/(\mu_i F_{n,i})\right] \quad (15)$$

From Eq.6 and 14 we can identify the components of the $\lambda_{4\times1}$ vector of Lagrange multipliers. The λ_1 and λ_2 are the tangential and normal wheel forces while λ_3 and λ_4 are the tangential and normal foot forces. Such a decomposition of the $\lambda_{4\times1}$ vector enables us to define the corresponding ratios.

In order to maintain point contact without slip at each contact two conditions have to be satisfied.

1) The normal force must be non-negative which implies,

$$F_{n,i} \geq 0 \qquad \forall\, i = 1,2 \quad (16)$$

2) Based on the Colombo model of friction we also arrive at the condition of no slip,

$$\left|F_{t,i}\right| \leq \mu_i \left|F_{n,i}\right| \qquad \forall\, i = 1,2 \quad (17)$$

In order to minimize the possibility of slippage and to minimize losses due to frictional forces we can choose to minimize the larger of the two force ratios. The optimization problem can be stated as,

$$\text{Minimize } \left[Max_{i=1,2}\ \{r_i^2\}\right] \quad (18)$$

subject to Eq.11, Eq.14-17 where q, v, and $\dot{v}$ are known or can be computed from the desired system motion.

It has been shown in the literature [21] that this kind of optimization problem has the solution $r_1^2 = r_2^2$ (19) in the absence of actuator constraints.

We use this result to provide us with an additional equation of constraint to append to the underdetermined system in Eq.12 and to solve for the unknown torques. The resulting solution is a quartic in the torques which has at most four feasible solutions. We choose the solution which can accomplish the motion with the smallest force ratio.

As we will see later in this paper, in the presence of actuator constraints the condition in Eq.19 is no longer optimal.

MODELING OF NONLINEARITIES

In our system we deal with two major nonlinearities, friction and actuator limits, which are artifacts present in any real world system. In our system, these nonlinearities have a marked effect on the system dynamics making their modeling imperative for any realistic simulation.

FRICTION

The dominant nonlinearity in the system is friction. Because of the complexity of the system it is difficult to develop analytical models of the friction. Instead, we assume a Coulomb like frictional law for the entire system and use experimental techniques to determine the coefficients.

A controlled experiment is set up for acquiring this data. A forward motion of 3.5 inches (0.0889 m) in 20 seconds (while maintaining a constant height of the CG) is commanded as shown in Figure 4.A. The wheel motors are turned off and the system uses only the powered legs for this maneuver. The foot forces (normal and tangential) for the motion are plotted in Figure 4.B.

Since the tangential inertial force is negligible for this motion we can directly use the obtained data for tangential

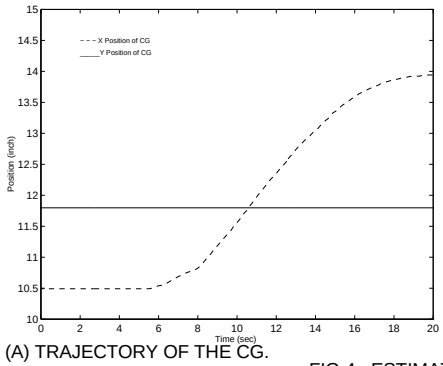

(A) TRAJECTORY OF THE CG.

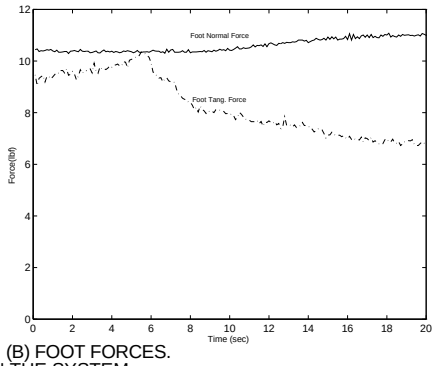

(B) FOOT FORCES.

FIG 4: ESTIMATION OF THE FRICTION IN THE SYSTEM.

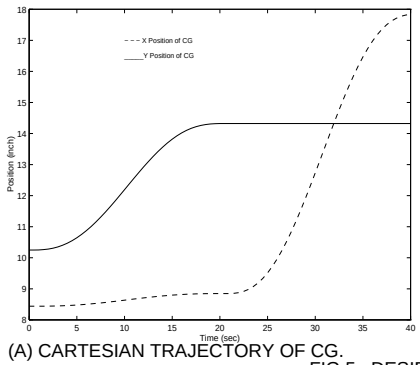

(A) CARTESIAN TRAJECTORY OF CG.

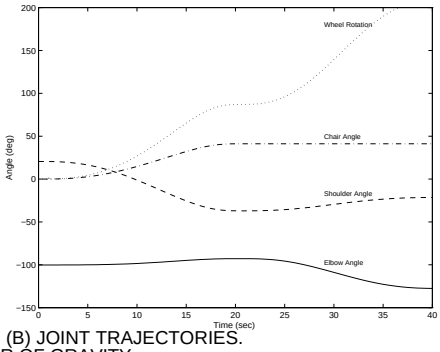

(B) JOINT TRAJECTORIES.

FIG 5: DESIRED MOTION OF THE CENTER OF GRAVITY.

force at the foot to characterize the friction in the system. The tangential force profile during the motion shows the characteristic peak in breakaway static friction which is overcome at about 6 seconds into the maneuver (as can be verified by the motion of X_{cg} in Figure 4.A). After the motion commences, we note that the tangential force value stabilizes to a constant value which gives us an estimate of the kinetic friction in the system.

While our experiment yields only the Cartesian frictional force (net sum of all friction of the system resolved in the Cartesian directions) it is adequate for our modeling and simulation purposes.

ACTUATOR LIMITS

The other nonlinearity present in our system is the presence of motor torque limits.

In any redundant system, the effect of the actuator reaching its limit is to reduce the degree of actuator redundancy present in the system. This is because the actuator under consideration will now be producing a determinate actuation force (equal to its limit). Hence, we can now eliminate this variable from the list of unknowns. In our system since the degree of actuator redundancy is one, if one actuator is saturated, the system becomes determinate and we rewrite Eq.12 as shown below,

$$\tau_{2\times 1} = \left(S^T \tilde{E}\right)^{-1}\left[(S^T M S)\dot{v} + S^T M \dot{S} v + S^T h\right] \qquad (20)$$

where $\tilde{E}_{6\times 2}$ is the modified torque distribution matrix (formed by setting the saturated torque to its limit in $E_{6\times 3}$ the initial torque distribution matrix).

TRAJECTORY GENERATION

The trajectory generation for our system is done to make the change in acceleration continuous at all times - the minimum jerk condition. This enforces the continuity of the trajectory in the acceleration, velocity and position levels. An added advantage of such a choice is that it provides for a smoother ride since it eliminates discontinuous changes in acceleration.

Thus, given the initial and final positions and zero initial and final velocities and accelerations we obtain two fifth order polynomials for the trajectories.
They are shown in dimensionless form below,

$$\bar{x} = 10\tau^3 - 15\tau^4 + 6\tau^5$$
$$\bar{y} = 10\tau^3 - 15\tau^4 + 6\tau^5 \qquad (21)$$

where $\bar{x} = \dfrac{x - x_0}{x_f - x_0}$, $\bar{y} = \dfrac{y - y_0}{y_f - y_0}$, $\tau = \dfrac{t}{T}$

These describe a minimum jerk Cartesian motion profile for the center of gravity of the chair.

Shown in Figure 5.A is the Cartesian position profile for the motion which lifts the front wheels of the wheelchair onto a fourteen inch step in two phases. The first phase consists of lifting the front wheels of the wheelchair 14 inches (0.3556 m) off the ground and moving it forward by 1 inch (0.0254 m) in 20 seconds. The second phase then moves the wheelchair a further 9 inches (0.2286 m) forward while maintaining the same height in the next 20 seconds. The resulting Cartesian trajectories are mapped back into the joint space using the inverse kinematics map and shown in Figure 5.B.

The Cartesian velocity and acceleration are determined

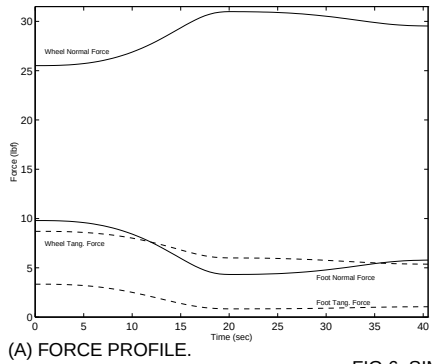

(A) FORCE PROFILE.

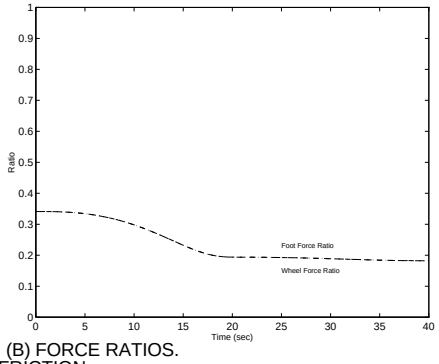

(B) FORCE RATIOS.

FIG 6: SIMULATION RESULTS WITH FRICTION.

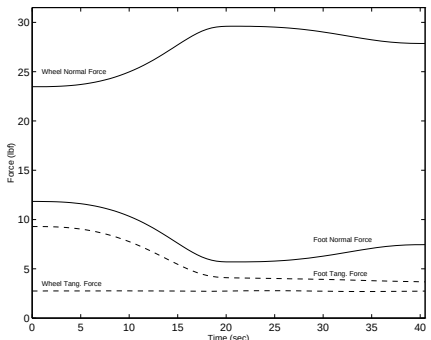

(A) WHEEL AND FOOT FORCES.

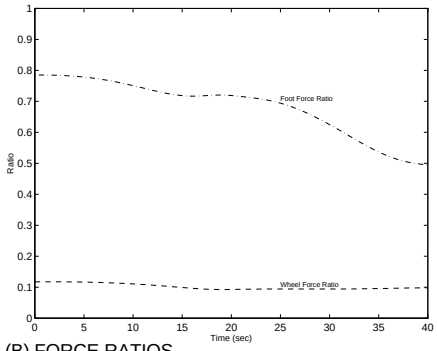

(B) FORCE RATIOS.

FIG 7: SIMULATION RESULTS WITH FRICTION AND ACTUATOR (WHEEL TORQUE) LIMITS.

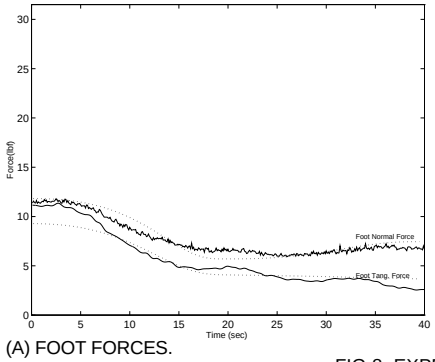

(A) FOOT FORCES.

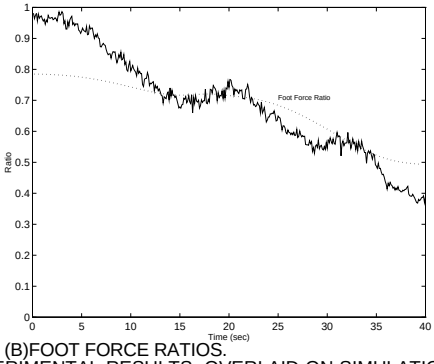

(B)FOOT FORCE RATIOS.

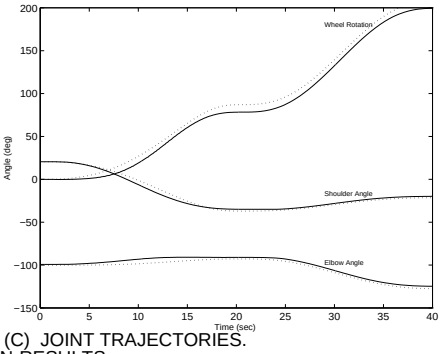

(C) JOINT TRAJECTORIES.

FIG 8: EXPERIMENTAL RESULTS OVERLAID ON SIMULATION RESULTS.

by differentiating the expression for position. Assuming rigid body motion, this process translates to continuity of acceleration change for every point in the task space. It also extends to continuity in the joint space because of the existence of a 1:1 inverse kinematics map. In this way any complex trajectory can be created by merging small pieces of trajectories while preserving continuity at the acceleration level.

SIMULATION RESULTS

The simulation studies were carried out for the motion described in Figure 5.

SYSTEM WITHOUT ACTUATOR LIMITS

The results presented in Figure 6 are for the case where there are no limits are imposed on the actuator torques but the friction is modeled in the system.

We observe again that for this sample motion the inertial tangential force due to the acceleration of the chair is negligible. The most significant component of the force is the friction in the system which opposes the force required to actually move the system.

SYSTEM WITH ACTUATOR LIMITS

In Figure 7, we present the case where there are actuator limits on the wheel motor. This solution to the system of equations is obtained in two stages. The first stage involves solution of the problem without imposing any actuator limits using the optimizing criterion developed earlier. The torques so obtained are checked for compatibility with the actuator limits. If the limit is violated we set that particular actuator force to its limit and then recompute the other actuator forces for the reduced order redundant system.

As mentioned earlier, since the degree of redundancy in our system is 1, the reduced redundancy system is now determinate and we solve for the other 2 torques using Eq.20.

When we contrast the scenarios with and without actuator limits we notice that in the first case the wheel provides a significant component of the tangential force and hence the saturation of the wheel torque has caused significant deviation from the equal force ratios condition.

We also note that since we now have a reasonably accurate model for the system we can vary the actuator limits. We observe that the solutions of such studies tend asymptotically towards the idealized optimal traction solution as the limit is raised.

EXPERIMENTAL RESULTS

The system is commanded to move according to the trajectory devised with the minimum jerk profile. The force histories obtained from the simulation (dotted) and observed experimentally (solid) are shown in Figure 8.A.

Figure 8.B depicts the comparison between the predicted force ratio at the foot and the actual force ratio. Figure 8.C depicts the comparison between the simulated (desired) trajectory and the actual trajectory. We note that the wheel motion lags considerably behind the desired value because of the lower bandwidth for control and the effects of actuator limiting. We also note that initially and when terminating the motion the system is slow to respond to the changes because of the low bandwidth of the wheel motor.

We observe that the experimental data agrees with the simulation. Because the experiments were performed with a rubber foot on a carpeted floor, we observe very large force ratios without any noticeable slip. The wheel normal force can only be inferred by subtracting the foot force from the weight (35.31 lbs) of the vehicle and is therefore not shown. The wheel tangential force is saturated at 2.74 lbs during the entire maneuver.

CONCLUDING REMARKS

The main focus of this paper was the traction optimization scheme for an actively controlled vehicle with legs and wheels that minimizes the tendency of the wheels and legs to slip. The optimization involves minimizing the largest force ratio among the locomotion elements. While it is theoretically possible to achieve the optimal condition in which all force ratios are equal, we found that in practice, saturation of the actuators and friction limits the performance of the system. We used experimental techniques to identify the friction and to develop models for actuator saturation. By constraining the optimization problem with these models, we were able to obtain optimal operating conditions for our system. We presented results that demonstrate the feasibility of our approach.

We also presented the design of our experimental prototype of a computer-controlled powered wheelchair with legs that is capable of navigating on uneven terrain. We note that another group independently arrived at a similar configuration for a hybrid vehicle for forestry applications [1]. The main direction for future work is to incorporate a posture regulation system (see, for example, [3]) that maintains the rider in a horizontal configuration (or any preferred orientation) even when the chair is climbing a step.

ACKNOWLEDGMENTS

This work was supported by the Whitaker Foundation by National Science Foundation Grants MSS-9157156, MIP-9420397, and CISE/CDA 88-22719. We thank Parris Wellman for helping with the design of the prototype and William Harwin for discussions relating to rehabilitation engineering design.

REFERENCES

[1] M. Hiller, and A. Kecskemethy, A computer-oriented approach for the automatic generation and solution of the equations of motion for complex mechanisms, *Proc. 7th World Congress on the Theory of Machines and Mechanisms*. Sevilla, 1987.

[2] S. Hirose, A study of design and control of a quadruped walking, *Int. J. Robotics Research*, Vol. 3, No. 2, pp. 113-133, 1984.

[3] S. Hirose, T. Sensu, and S. Aoki, The TAQT carrier: A practical terrain-adaptive quadru-track carrier robot, *Proceedings IEEE/RSJ Int. Conf. Intelligent Robots and Systems*, Raleigh, NC, pp. 2068-2073, July, 1992.

[4] N. Hogan, Impedance control: Parts I, II, *J. Dynamic Systems, Measurement and Control*, Vol. 107, pp: 1-16, March 1985.

[5] T. Houston, and R. Metzger, Combination wheelchair and walker apparatus, U.S. *Patent* 5, 137, 102, Aug. 11, 1992.

[6] V. Kumar, and K. J. Waldron, Actively coordinated mobility systems, *ASME J. Mechanisms, Transmissions and Automation in Design*, 111 (2), pp. 223-231, 1989.

[7] A. McLaurin, and P. Axelson, Wheelchair standards: an overview, *J. Rehabilitation Research and Development Clinical Supplement* (2): 100-103, 1990.

[8] R. S. Mosher, Exploring the potential of a quadruped, *Int. Automotive Eng. Congress*, SAE Paper no. 690191, Detroit, Mich., Jan. 1969.

[9] P. D. Nisbet, J. P. Odor, and I. R. Louden, The CALL Centre smart wheelchair, *First Int. Conf. on Robotics Apps. in Medical and Healthcare*, Ottawa, 1988.

[10] D. E. Okhotsimski, V. S. Gurfinkel, E. A. Devyanin, and A. K. Platonov, Integrated walking robot development, *Machine Intelligence*, Vol. 9. Eds. J. E. Hayes, D. Michie, and L. J. Mikulich, 1977.

[11] E. Peizer, and D. W. Wright, Five years of wheelchair evaluation. *Veterans Administration Prosthetics Center*. New York, NY, 1969.

[12] M. H. Raibert, *Legged Robots that Balance*. MIT Press. Cambridge. Massachusetts. 1985.

[13] M. W. Thring, *Robots and Telechairs: Manipulators with Memory, Remote Manipulators, Machine Limbs for the Handicapped*. Ellis Horwood; New York: Halsted Press, 1983.

[14] N. Ulrich, and V. Kumar, Mechanical design methods of improving manipulator performance. *Proceedings of the 5th Int. Conf. Advanced Robotics*, Pisa, pp. 515-520, June 1991.

[15] D. R. Voves, J. F. Prendergast, and T. J. Green, Stairway chairlift mechanism, *U.S. Patent* 4,913,264, April, 1990.

[16] H. Wakaumi, K. Nakamura, and T. Matsumura, Development of an automated wheelchair guided by a magnetic ferrite marker lane. *J. Rehab. Res. and Dev.* 29 (1) 1992.

[17] K. J. Waldron, V. J. Vohnout, A. Pery, and R. B. McGhee, Configuration design of the adaptive suspension vehicle. *Int. J. Robotics Research*. 3(2), pp. 37-48, 1984.

[18] P. Wellman, V. Krovi, and V. Kumar, An adaptive mobility system for the disabled. 1994 *IEEE Int. Conf. Robotics Automation*, pp. 2006-2011, May 8-13, 1994.

[19] P. Wellman, A hybrid mobility system., *Masters Thesis*. Department of Mechanical Engineering and Applied Mechanics, University of Pennsylvania, 1994.

[20] C-D Zhang, and S. M. Song, Gaits and geometry of a walking chair for the disabled, *J. Terramechanics*, 26(314), pp. 211-233, 1989.

[21] L. Johnson, V. Kumar, and J. F. Gardener, Optimization of Contact Forces in Multi-fingered and Multi-legged Robots. *2nd Ann. Applied Mechanisms and Robotics Conference*. V2. 1991.